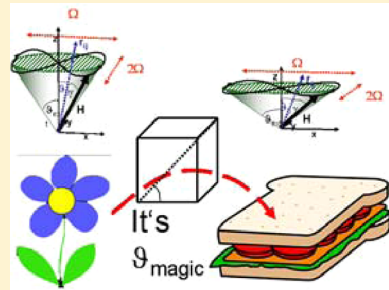


Magnetic Field Controlled Composite Paramagnetic–Diamagnetic Colloidal Phases

A. Ray and Th. M. Fischer*

Institut für Experimentalphysik, Universität Bayreuth, 95440 Bayreuth, Germany

ABSTRACT: We report on differently ordered colloidal phases of a mixture of paramagnetic and diamagnetic colloids subject to a quickly varying time dependent magnetic field. Effectively paramagnetic and effectively diamagnetic colloids are created from paramagnetic and nonmagnetic colloids immersed into a thin film of aqueous ferrofluid. The time-averaged dipole interaction between induced dipoles can be characterized by a uniaxial external precession angle and a biaxial eccentricity characterizing the anisotropy of the external field modulation. The variation of both control parameters causes a sequence of transitions between differently correlated orientation order between the paramagnetic and diamagnetic colloids. We observe the formation of bonds between paramagnets and diamagnets along one or two directions with a staggered order of the magnetic moments. Bonds between similar particles with uniform order of the magnetic moments form along directions orthogonal to bonds between different particles along the staggered directions. When the external precession angle passes the magic angle, the particle order rearranges and staggered directions with bonds between different particles change into uniformly ordered directions with bonds between similar particles and vice versa. The transition in order occurs in two steps with a biaxial phase intervening between the two uniaxial ordering phases.



1. INTRODUCTION

Neutralization of opposite charges is one of the driving concepts leading to the organization of matter on the atomic and molecular scale. The interaction between point charges is isotropic and does not depend on direction. It is spontaneous breaking of rotational symmetry and the quantization of angular momentum that nevertheless produces crystalline structures with directed bonds in atoms and molecules. Colloidal particles have been used as a model for atoms on a larger scale.^{1,2} They are, however, of mesoscopic size, where quantum phenomena are absent, and angular momentum is a continuous quantity. The principles leading to directed bonds in microscopic systems therefore do not work on the colloidal scale. In isotropically interacting colloids, the energy of interaction does not depend on the bond direction. Steric interactions, that is, the hard-core repulsion between two colloids, are isotropic interactions that create an excluded volume along an arbitrary direction that further particles may not enter. Spontaneously breaking of the continuous rotational symmetry via steric interactions is the mechanism to form a colloidal crystal³ with reduced discrete rotational symmetry. The only possibility of obtaining directed anisotropic bonds in colloidal systems is by using colloidal particles that are intrinsically anisotropic. For this reason, chemists have synthesized Janus particles^{4,5} and patchy colloids^{6,7} with surface functionalities that vary as a function of the location on the particle surface. Other possibilities are the use of ellipsoidal particles^{8–10} the shape of which is different in different directions. A third possibility is to use a magnetic¹¹ or electric¹² dipole moment using an external magnetic or electric field. Induced paramagnetic dipoles do not neutralize in an external field but build up an

induced magnetization with a macroscopic magnetic moment given by the magnetization of the sample times its volume. The situation changes when considering a mixture of paramagnetic and diamagnetic colloids.¹³ Diamagnets and paramagnets point into opposite directions in the same field. They are able to neutralize each other on a macroscopic scale in the sense that the net dipole moment per unit cell within the lattice is decreased and possibly canceled entirely given the right set of conditions. In this sense, mixtures of paramagnets and diamagnets in an external magnetic field are a model system for neutralizing anisotropically interacting particles that possess a variety of mesoscopic arrangements that are richer than that of isotropic colloids and than that of non-neutralizing anisotropic colloids. In the current manuscript, we show a few of the most obvious colloidal phases that form in such a system, when we apply a field varying on time scales faster than the interparticle dynamics.

The remainder of this work is organized as follows. Section 2 gives a sketch of the experiments on paramagnetic colloids and diamagnetic holes in ferrofluids. Section 3 explains the time-averaged dipolar interaction between the particles and derives the uniaxial and biaxial contribution to the time-averaged interaction. A parameter α is introduced that controls the ratio of both interactions. Section 4 shows the experimentally observed order of the particles, while section 5 discusses the different phases in the framework of section 3. Finally, the conclusions are presented in section 6.

Received: December 19, 2011

Revised: June 19, 2012

Published: June 21, 2012

2. EXPERIMENT

In our experiment, we have used micrometer-sized superparamagnetic particles of diameter $2.8\text{ }\mu\text{m}$ (Invitrogen Dynal Oslo, Norway) and fluorescence red polystyrene particles of diameter $1.0\text{ }\mu\text{m}$ (Thermo Scientific). We used a water-based ferrofluid EMG 707 from FerroTec Ferrosound (FerroTec GmbH, Germany). The susceptibility provided by the supplier was $\chi_f = 1.5$; however, our results could be fitted best with a value of $\chi_f = 2.1$, which we use throughout this work. Both the superparamagnetic and fluorescence polystyrene particles were immersed in undiluted ferrofluid with controlled proportions and were placed between two coverslips. The sandwiched coverslips were placed in a time-dependent magnetic field produced by five coils (two coils for the x direction, two coils for the y direction in the plane of the ferrofluid film, and one z coil normal to the film) and were observed with either reflection or fluorescence microscopy (LEICA DM5000, Leica Microsystems Wetzlar GmbH, Germany, Figure 1a)

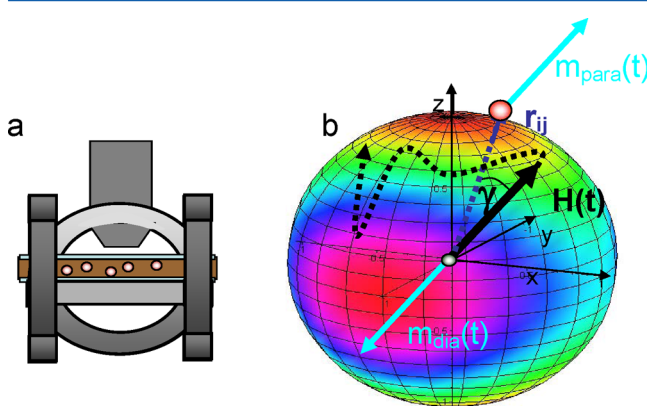


Figure 1. (a) Scheme of the experimental setup. The sample of ferrofluid is sandwiched between two glass slides. Solenoids for the x , y , and z directions surround the sample that is observed through the objective of a microscope. (b) Scheme of a time-dependent field $H(t)$ and the magnetic moments m_{dia} and m_{para} of a diamagnetic and a paramagnetic bead separated from each other by the vector r_{ij} . The color-coded sphere shows the second moment of the time distribution of the magnetic field directions. Directions in which the magnetic field points more frequent than average are colored in orange, averagely frequented directions are shown in cyan, and less than average frequented field directions are shown in red. The color coding also coincides with the character of the interaction for the bond vector r_{ij} between both particles. For a diamagnetic and paramagnetic particle, orange bond directions are repulsive, cyan directions are indifferent, and red directions are attractive. Attraction converts into repulsion and vice versa for particles of the same sort.

Typical fluxes in one direction were about 3 mT and orientational fluctuations of the magnetic field were about $f = \Omega/2\pi = 10\text{--}40\text{ Hz}$. At these conditions, the viscous forces inhibit the motion of individual particles into their instantaneous equilibrium positions and only the time-averaged dipolar interactions between the particles force them into their time-averaged equilibrium conformation. At the ferrofluid/glass interface, the magnetic boundary conditions (continuity of B_\perp and H_\parallel^{14}) cause a deflection of the field. The field direction of the magnetic field changes from the air into the ferrofluid film according to $\hat{H}_\perp^{\text{ferrofluid}} = \hat{H}_\perp^{\text{air}}/(1 + \chi_f)$ and $\hat{H}_\parallel^{\text{ferrofluid}} = \hat{H}_\parallel^{\text{air}}$, and the orientation angle in the ferrofluid and in the air are related via $\tan \theta_{\text{ferrofluid}} = (1 + \chi_f)\tan \theta_{\text{air}}$. $\chi_f = 2.1$ denotes the magnetic

susceptibility of the ferrofluid. If not stated otherwise, external fields and external orientations are given in terms of their values inside the ferrofluid.

3. TIME-AVERAGED DIPOLE INTERACTIONS

The magnetic field induces excess magnetic moments $\mathbf{m}_i(t)$ in the particles that interact via the dipole–dipole interaction

$$W_{ij} = -\frac{\mu_0}{4\pi} \mathbf{m}_i(t) \mathbf{m}_j(t) : \frac{3\mathbf{r}_{ij}\mathbf{r}_{ij} - r_{ij}^2 \mathbf{I}}{r_{ij}^5} \quad (1)$$

, where μ_0 denotes the vacuum permeability, \mathbf{r}_{ij} denotes the separation vector between the interacting beads, and \mathbf{I} denotes the unit tensor. For longitudinal orientations with both magnetic moments aligned parallel along the separation vector, this interaction is attractive while transversal orientations of magnetic moments aligned perpendicular to the separation vector are repulsive. If on average the orientation of the aligned magnetic moments is in an arbitrary orientation with respect to the separation vector, we have an isotropic time distribution. For such isotropic time distribution, the attractive and repulsive orientations cancel each other. This cancellation occurs because the tensor $(3\mathbf{r}_{ij}\mathbf{r}_{ij} - r_{ij}^2 \mathbf{I})/(r_{ij}^5)$ is traceless, that is, its contraction with the unit tensor vanishes. The expression in eq 1 does not change if we replace the tensor $\mathbf{m}_i\mathbf{m}_j$ by its traceless part $\mathbf{m}_i\mathbf{m}_j - \frac{1}{3}(\mathbf{m}_i \cdot \mathbf{m}_j)\mathbf{I}$. Hence, only the traceless part $\mathbf{m}_i\mathbf{m}_j - \frac{1}{3}(\mathbf{m}_i \cdot \mathbf{m}_j)\mathbf{I}$ of the tensor $\mathbf{m}_i\mathbf{m}_j$ that measures the deviation of the magnetic moment orientation from isotropic is relevant for the interaction between the beads. If we neglect the influence of other beads on the excess magnetic moment of an individual bead and if we assume an instantaneous response of the bead magnetization, then the magnetic moment is related to the external field via

$$\mathbf{m}_i = \Delta\chi_{\text{eff}}^i V_i \mathbf{H}_{\text{ext}} \quad (2)$$

where

$$\Delta\chi_{\text{eff}}^i = \frac{3(1 + \chi_f)(\chi_i - \chi_f)}{1 + \chi_i + 2(1 + \chi_f)} \quad (3)$$

is the effective susceptibility contrast of the particle of susceptibility χ_i and volume V_i to the ferrofluid with susceptibility χ_f . The dipole interaction can therefore be rewritten as

$$W_{ij} = -\frac{\mu_0 \Delta\chi_{\text{eff}}^i \Delta\chi_{\text{eff}}^j V_i V_j}{4\pi} \frac{3\mathbf{r}_{ij}\mathbf{r}_{ij} - r_{ij}^2 \mathbf{I}}{r_{ij}^5} : \left[\mathbf{H}_{\text{ext}}(t) \mathbf{H}_{\text{ext}}(t) - H_{\text{ext}}^2(t) \frac{\mathbf{I}}{3} \right] \quad (4)$$

The dimensionless Mason number $M = \eta\Omega/\mu_0\chi^2 H^2$ characterizes the ratio of viscous versus magnetic interactions,¹⁵ where $\eta = 10^{-3}\text{ Nsm}^{-2}$ denotes the water viscosity, and Ω denotes the modulation frequency of the magnetic field. The viscous dissipated power $P_{\text{visc}} \propto \eta r^3 \omega$ of a bead moving at a rate ω and distance r around another bead cannot exceed the driving magnetic power $P_{\text{magn}} \propto r a^2 \mu_0 \Delta\chi^2 H^2 \Omega$ of the beads of radius a such that the shear rates ω must be always smaller than $\omega < \Omega(a^2/r^2)M^{-1}$. At the conditions used here, the Mason number is large $M > 1$ and the motion of the beads is with a lower rate $\omega < \Omega$ than the magnetic field for any separation $r > a$ of the beads. Because in our experiments the intraparticle dynamics is

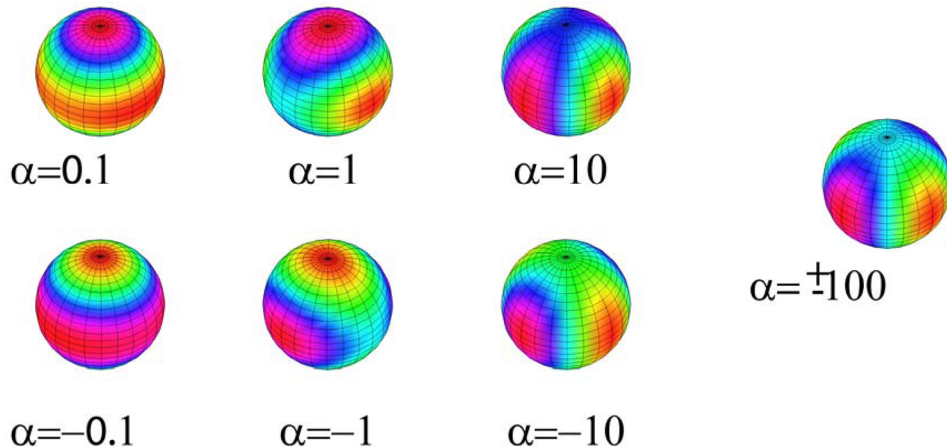


Figure 2. Bond direction dependence of the time-averaged dipolar interactions color coded (violet = attractive via, cyan = indifferent toward, orange = repulsive) for different values of α . The eigenvalues switch sign for $\alpha = 1$ for the x direction, for $\alpha = 0, \pm\infty$ for the uniaxial z direction, and for $\alpha = -1$ for the y direction.

slow compared to the modulation of the external field, the particle separations can be considered time independent during one period of the magnetic field such that the time average taken over one period affects only the traceless magnetic field tensor $\mathbf{H}_{\text{ext}}(t)\mathbf{H}_{\text{ext}}^*(t) - H_{\text{ext}}^2(t)(1/3)$. For a modulation of the form

$$\mathbf{H}(t) = \hat{H}_z \mathbf{e}_z + \hat{H}_x \mathbf{e}_x \sin \Omega t + \hat{H}_y \mathbf{e}_y \sin 2\Omega t \quad (5)$$

The time-averaged traceless dyadic product of the external field is diagonal in x, y, z coordinates and reads

$$\begin{aligned} & \mathbf{H}_{\text{ext}}(t)\mathbf{H}_{\text{ext}}^*(t) - H_{\text{ext}}^2(t)\frac{\mathbf{I}}{3} \\ &= -\frac{\hat{H}_{\text{ext}}^2}{3}P_2(\cos \vartheta_{\text{ext}})\mathbf{U} + \frac{\varepsilon \hat{H}_{\text{ext}}^2}{6}P_2^2(\cos \vartheta_{\text{ext}})\mathbf{B} \end{aligned} \quad (6)$$

where $\mathbf{U} = \mathbf{e}_x\mathbf{e}_x + \mathbf{e}_y\mathbf{e}_y - 2\mathbf{e}_z\mathbf{e}_z$, and $\mathbf{B} = \mathbf{e}_x\mathbf{e}_x - \mathbf{e}_y\mathbf{e}_y$ are the uniaxial and biaxial traceless matrices. $\hat{H}_{\text{ext}}^2 = \overline{H_{\text{ext}}^2(t)}$, $\cos \vartheta_{\text{ext}} = (\hat{H}_z)/(\hat{H}_{\text{ext}})$ is the time-averaged precession angle and $\varepsilon = (\hat{H}_x^2 - \hat{H}_y^2)/(\hat{H}_x^2 + \hat{H}_y^2)$ is the eccentricity of the modulation. Insertion of eq 6 into 4 leads to the time-averaged dipolar interaction in the form

$$\begin{aligned} \bar{W}_{ij} = & -\frac{\mu_0}{2\pi} \frac{\Delta\chi_{\text{eff}}^i V_i \Delta\chi_{\text{eff}}^j V_j \hat{H}_{\text{ext}}^2}{(r_{ij})^3} \left[P_2(\cos \vartheta_{\text{ext}})P_2(\cos \vartheta_b) \right. \\ & \left. + 2\varepsilon \frac{(2-2)!}{(2+2)!} P_2^2(\cos \vartheta_{\text{ext}})P_2^2(\cos \vartheta_b) \cos(2\varphi_b) \right] \end{aligned} \quad (7)$$

where ϑ_b and φ_b are the bond tilt and azimuth angle defined via $\cos \vartheta_b = z/r$ and $\sin \varphi_b = y/(r \cos \vartheta_b)$ and $P_2(x)$ and $P_2^2(x)$ are Legendre polynomials of degree 2 and associated Legendre polynomials of degree 2 and order 2. For vanishing eccentricity of the modulation, the averaged dipole interaction is purely uniaxial, and the interaction only depends on the bond tilt angle. The averaged dipole interaction changes sign at the magic angle $\vartheta_b = \vartheta_{\text{magic}}$, that is, the zero of the second Legendre polynomial. In magic angle spinning NMR, this magic angle ϑ_{magic} is used to suppress the influence of dipole interactions on NMR line shapes. Here, it is used in a similar way to switch the sign of the average dipole–dipole interactions. From eq 6, we deduce that there are three ways to switch the sign. The product of the effective susceptibility contrasts $\Delta\chi_{\text{eff}}\Delta\chi_{\text{eff}}^*$ is

positive for similar beads but negative for a paramagnetic and diamagnetic pair of beads. Bond directions that are attractive for similar beads are repulsive for a paramagnetic and diamagnetic pair of beads and vice versa. We might switch the sign by using precession angles of the magnetic field $\vartheta_{\text{ext}} > \vartheta_{\text{magic}}$ below and above the magic angle. Finally, the interaction switches sign when the bond tilt angle between the beads is $\vartheta_b < \vartheta_{\text{magic}}$ below and above the magic angle.

With eccentricity, the bond structure becomes biaxial and the bond direction dependence of the interaction is entirely controlled by the parameter $\alpha = [le|P_2^2(\vartheta_{\text{ext}})]/[P_2(\vartheta_{\text{ext}})] = (3l H_x^2 - H_y^2)/(H_x^2 + H_y^2 - 2H_z^2)$. The biaxiality is of minor importance if the precession angle of the field is far away from magic $|\alpha| < 1$ because then the uniaxial components overpower the biaxiality. Close to the magic angle, however, the eigenvalue structure of the dyadic product of the magnetic field changes such that one eigenvalue is zero while the other two have opposite signs. This results in one attractive, one repulsive, and one indifferent bond direction.

In Figure 2, we plot the color-coded bond angular dependence of the averaged dipole interaction for similar beads as a function of α . For external precession angles far above the magic angle $0 < \alpha \ll 1$, the cyan color at the latitude of the magic bond tilt angle separates the attractive polar bond directions (blue-violet) from the repulsive directions around the equator. When approaching the magic precession angle, the indifferent (cyan) zone approaches the equator near $\varphi_b = 0, \pi$ and remains near the magic bond tilt angle for intermediate longitudes. The indifferent zones from the southern and northern hemispheres eventually merge for $\alpha = 1$ when the eigenvalue in the x direction switches sign restricting the repulsive directions around the equator to the longitudes around $\varphi_b = \pm\pi/2$. When further approaching the magic precession angle $\alpha = 10$, the merged indifferent zones disjoin into an eastern and western zone creating an attractive plane along $\varphi_b = 0, \pi$. Then, the indifferent zone moves toward the poles near the longitudes around $\varphi_b = \pm\pi/2$, where they merge right at the magic precession angle $\alpha = \pm\infty \approx \pm 100$. It is at the magic precession angle where the eigenvalue in the z direction switches sign leaving an attractive direction along the x axis and a repulsive direction along the y axis. When passing the magic precession angle, the indifferent zones disjoin and retreat along $\varphi_b = 0, \pi$ ($\alpha = -10$). The plane $\varphi_b = \pm\pi/2$ is now repulsive.

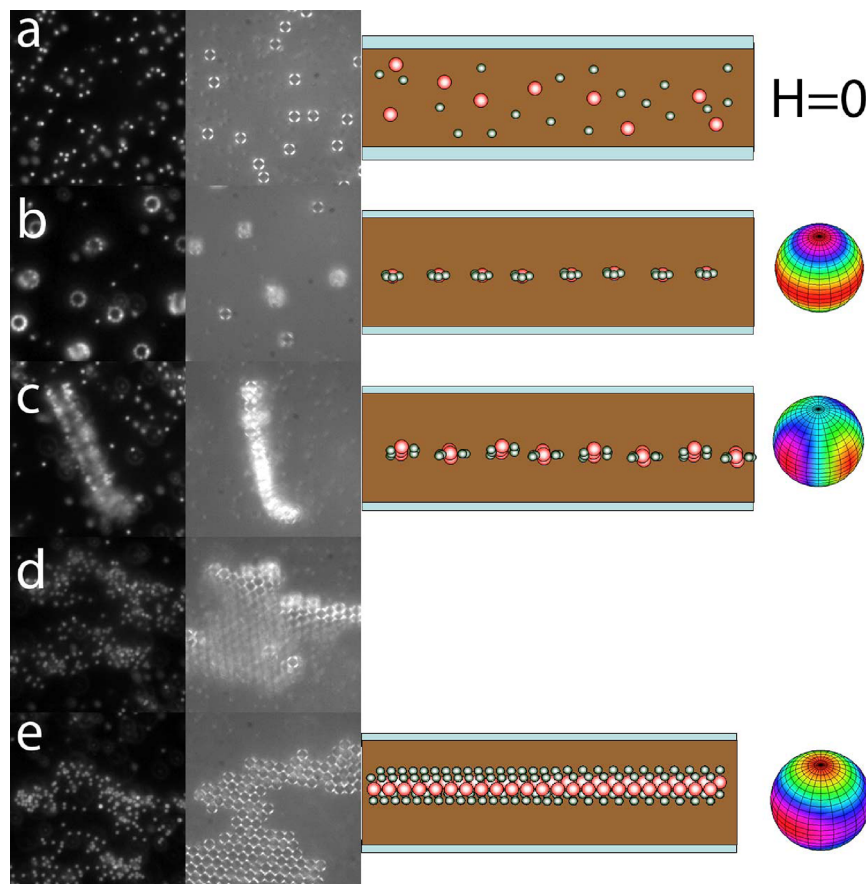


Figure 3. Collection of fluorescence (left) and polarization reflection microscope images (middle left) together with a side-view scheme of the structure (middle right) of a mixture of paramagnetic beads $2a_p = 2.8 \mu\text{m}$ and effective diamagnets $2a_d = 1.0 \mu\text{m}$ immersed into an undiluted aqueous ferrofluid $\chi_f = 2.1$. Fluorescence microscopy images (left) visualize the diamagnets while polarization reflection images (second from the left) visualize the paramagnets. The right figure shows the corresponding angular dependence of the dipole interactions as explained in Figure 2. (a) Random arrangement in the absence of a magnetic field. (b–d) Recorded in a magnetic field of $H_{||} = [(\hat{H}_x^2 + \hat{H}_y^2)/2]^{1/2} = 1.82 \text{ mT}$ and a frequency $\Omega = 120 \text{ s}^{-1}$. The vertical field (precession angle and α computed with $\chi_f = 2.1$) in the images were b, $H_z^{\text{air}} = 26.5 \text{ mT}$ ($\vartheta_{\text{ext}} = 12^\circ$, $\alpha = 0.002$); c, $H_z^{\text{air}} = 4.0 \text{ mT}$ ($\vartheta_{\text{ext}} = 54, 73^\circ$, $|\alpha| > 200$); d, $H_z^{\text{air}} = 2.22 \text{ mT}$ ($\vartheta_{\text{ext}} = 68^\circ$, $\alpha = -0, 14$); e, $H_z^{\text{air}} = 1.27 \text{ mT}$ ($\vartheta_{\text{ext}} = 77^\circ$, $\alpha = -0.1$).

Finally, the indifferent zones merge at the equator near $\varphi_b = \pm\pi/2$, the third eigenvalue along the y axis switches sign ($\alpha = -1$), and the indifferent zone disjoins to move back to the magic bond tilt angle with a polar repulsive direction and an equatorial attractive direction that is just opposite to the behavior observed for a precession angle below magic ($\alpha = -0.1$). The effect of the eccentricity is, hence, a sequential change of sign of the three eigenvalues instead of a simultaneous switch for a truly uniaxial modulation. The same result holds for a paramagnetic and a diamagnetic bead when we interchange attractive and repulsive.

It is therefore clear that the use of time-dependent magnetic fields varying in all three directions of space open up the possibility to create a rich variety of differently arranged assemblies of colloids. The use of paramagnets and diamagnets further enriches the possibilities since bond directions between magnetically similar and different particles point along directions that are orthogonal to each other. Some of those assemblies are shown in the next section.

4. RESULTS

We applied a field of the form eq 5 with an eccentricity of less than 5%. This ensures that the dyadic product of the magnetic field at two different times is a symmetric tensor ($\overline{\mathbf{H}(t)\mathbf{H}(t')} =$

$\mathbf{H}(t')\mathbf{H}(t) = \mathbf{0}$), where the bar denotes the time average. As a consequence, there is no net time averaged torque onto the colloidal structure.¹⁶ In what follows, we describe the assemblies of paramagnetic and diamagnetic particles as we increase the angle ϑ_{ext} .

Colloidal Flowers. In a static field $\hat{H} = 21\,200 \text{ A/m}$, $\vartheta_{\text{ext}} = 0$ normal to the ferrofluid film, we observe the formation of colloidal flowers. Such flowers form because of the dipolar attraction of diamagnetic particles in the equatorial plane $\vartheta_b = \pi/2$ of the paramagnets. They were first discovered by Erb et al.¹³ They are highly dynamic structures where the petals of the flowers may diffuse,¹⁷ and they can be easily set into rotation with time-dependent magnetic fields having an asymmetric part in the dyadic product.¹⁸ Figure 3b shows a fluorescence micrograph of such colloidal flowers with $2a_p = 2.8 \mu\text{m}$ paramagnetic cores and $2a_d = 1.0 \mu\text{m}$ petals. An ensemble of flowers can be seen via the fluorescent petals of the flower surrounding the nonfluorescent paramagnetic cores. The flowers are located in the middle of the sample indicating that gravitation and image dipoles prevent the binding of paramagnetic beads into one-dimensional strings with a diamagnetic mantle. Different flowers in the ensemble are distributed at an approximately nearest neighbor distance of 6–12 μm .

Decorated Strings. Upon increasing the precession angle to $\vartheta_{\text{ext}} = \vartheta_{\text{magic}}$, we observe the formation of paramagnetic strings undulating around the middle plane of the film with a period of three to five beads (Figure 3c). The entire structure is decorated with a collection of diamagnets that horizontally adsorb to the undulating string at the sides of the string. The bonds between diamagnets and paramagnets in this structure are also in the horizontal plane but are perpendicular to the bonds between the paramagnets in the string. A scheme of the decorated strings is shown to the right of Figure 3c. These strings correspond to the biaxial angular dependence of the dipolar interactions.

Sandwiched Membranes. At precession angles of about $\vartheta_{\text{ext}} = 68^\circ$, the paramagnetic beads form membranes instead of strings. These paramagnetic membranes are sandwiched between two layers of diamagnets that are adsorbed to the membrane on either side. At the transition angle $\vartheta = 58^\circ$, the orientation of the membrane normal is in the plane of the ferrofluid making the sandwich structure clearly visible in the fluorescence microscope image. The two diamagnetic adsorption layers appear as brightly fluorescing lines of diamagnetic beads sandwiching the nonfluorescent paramagnets. Upon increasing the precession angle, the membrane bends (Figure 3d) such that part of the membrane normal remains in the horizontal direction while the normal to the lower part of the membrane now aligns with the film normal. Eventually upon further increasing the precession angle, the membrane flattens and entirely lies in the film plane (Figure 3e) allowing a closer inspection of the diamagnetic order of the absorbed layers. For all systems studied here, the paramagnetic membrane is a close-packed two-dimensional structure with a hexagonal unit cell with unit vectors having the length of a paramagnetic bead diameter $2a_p$. The order of the diamagnetic adsorbate, on the contrary, varies a lot and sensitively depends on the size of the diamagnetic beads, on the concentration ratio of diamagnets versus paramagnets, and on the susceptibility of the diluted background ferrofluid. In what follows, we describe the order of the diamagnetic adsorbate under various conditions.

Paramagnetic Crystal Enslaved Diamagnetic Gas Phase. Figure 3e shows a fluorescence and a reflection microscope image of the same sample taken immediately one after another for a tilt angle of $\vartheta_{\text{ext}} = \pi/2$. The paramagnetic particles order into a series of planar clusters surrounded by regions that are completely depleted of paramagnetic colloids. Within the clusters, a crystalline hexagonal arrangement of the paramagnetic beads is observed. The arrangement of the diamagnetic colloids is not completely uncorrelated to the paramagnets. Diamagnetic particles from the paramagnetic-depleted regions adsorb on top and below the paramagnetic crystalline clusters. As a result, the density of diamagnetic particles on top and below the clusters is larger than the density in the paramagnetic-depleted regions. The paramagnetic crystal is sandwiched between two layers of diamagnetic gas. The diamagnetic particles perform Brownian motion, and the mean-square displacement of the diamagnets increases linearly (Figure 4) with a slope defining the gaseous diffusion constant of the diamagnets. The increase of the mean-square displacement beyond the area of the unit cell of the paramagnetic crystal shows that the diamagnets remain mobile in this phase. For this reason, we call this phase the paramagnetic crystal enslaved diamagnetic gas phase. This does not mean that the diamagnetic gas possesses no order. In Figure 5, we plot the radial correlation functions $g_{dd}(r)\Delta r = [1/(2N_d^2)]\sum_{i,j}\int_r^{r+\Delta r} dr \delta(r - |\mathbf{r}_{id} - \mathbf{r}_{jd}|)$

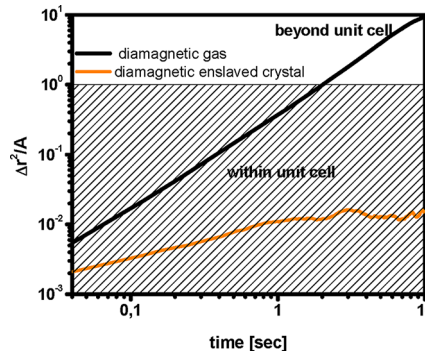


Figure 4. Mean-square displacement of the diamagnetic beads upon a cluster for a diamagnetic gas $H_z = 0.8$ mT, $\Omega = 120$ s $^{-1}$, $H_{||} = 1.82$ mT, $2a_d = 1$ μm (black) and for an enslaved crystal $H_z = 1.01$ mT, $\Omega = 120$ s $^{-1}$, $H_{||} = 1.82$ mT, $2a_d = 2$ μm (orange). The shaded region corresponds to mean-square displacements smaller than the paramagnetic unit cell size.

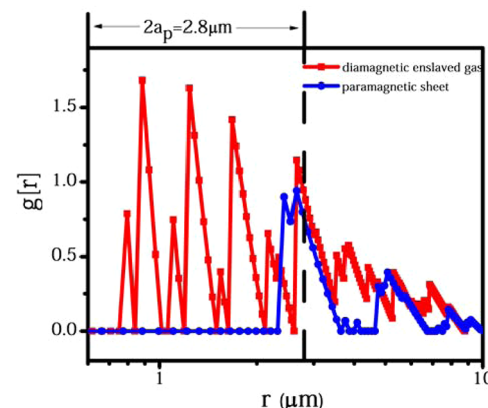


Figure 5. Radial correlation function of paramagnetic particles (blue) and diamagnetic particles (red) in a diamagnetic gaseous phase cluster. Although the diamagnetic gas is mobile, the crystal structure of the paramagnets is imprinted upon the diamagnets.

$-|\mathbf{r}_{id} - \mathbf{r}_{jd}|)$ and $g_{pp}(r)\Delta r = [1/(2N_p^2)]\sum_{i,j}\int_r^{r+\Delta r} dr \delta(r - |\mathbf{r}_{ip} - \mathbf{r}_{jp}|)$ of the paramagnets and diamagnets, where N_p and N_d are the number of paramagnets and diamagnets in a particular cluster, and the \mathbf{r}_{ip} and \mathbf{r}_{jd} are the positions of the i th paramagnet and the j th diamagnet. While the long-range behavior of both correlation functions is governed by the shape of the cluster, the short-range behavior shows that despite the mobility of the diamagnetic gas, the crystal order of the paramagnet is imprinted upon the gas via the magnetic field modulations from the paramagnet.

The autocorrelation function of the diamagnets share the peaks occurring in the autocorrelation function of the paramagnets. Because the diameter of the diamagnets is much smaller than that of the paramagnets, more than one diamagnet can reside on top and below one paramagnet. We observe a disorder in the occupancy number of the diamagnets of the sites above and below the paramagnetic crystals. A site can be vacant or have one, two, three, or four diamagnets on top of a paramagnet. This disorder is expressed by the substructure in the cross correlation function occurring in the hard-core region of the paramagnets of the auto correlation function of the diamagnets.

Paramagnetic Crystal Enslaved Diamagnetic Crystal Phase. Upon increasing the radii of the diamagnets and upon

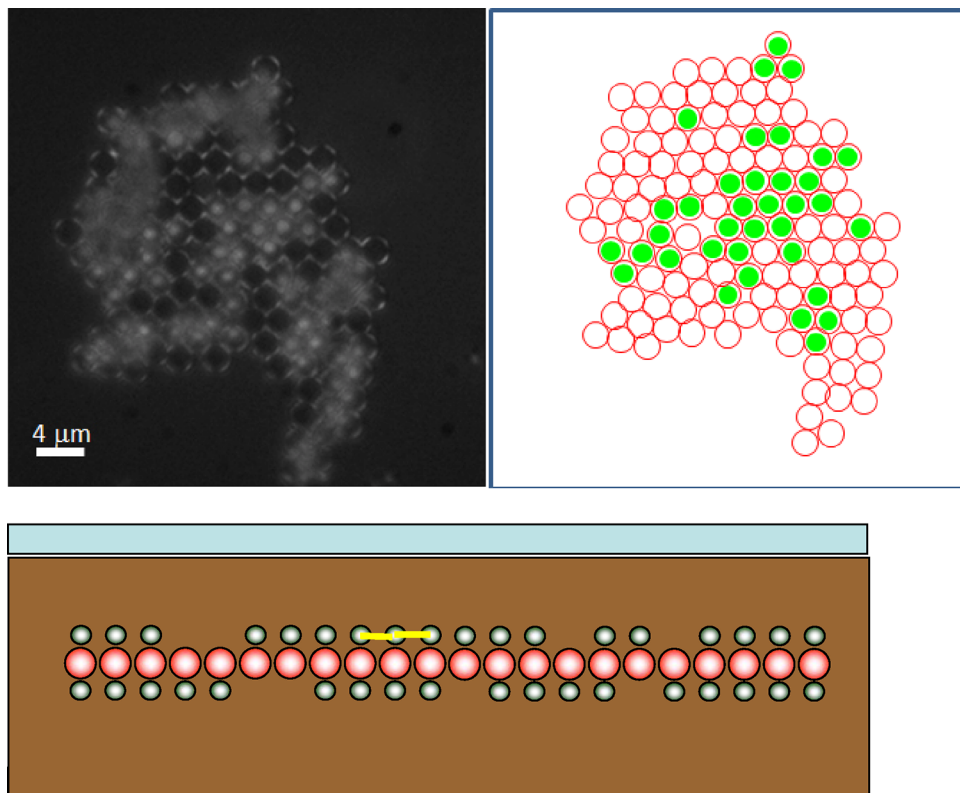


Figure 6. (top left) Polarization reflection microscope image of an enslaved crystalline phase of the diamagnets recorded at $H_z = 1.01$ mT, $\Omega = 120$ s^{-1} , $H_{\parallel} = 1.82$ mT, $2a_d = 2.0$ μm . The magnetic holes are sitting on top of the paramagnets as sketched in the scheme to the top right. The scheme at the bottom shows a side view with two of the frustrated bonds between the diamagnets shown in yellow.

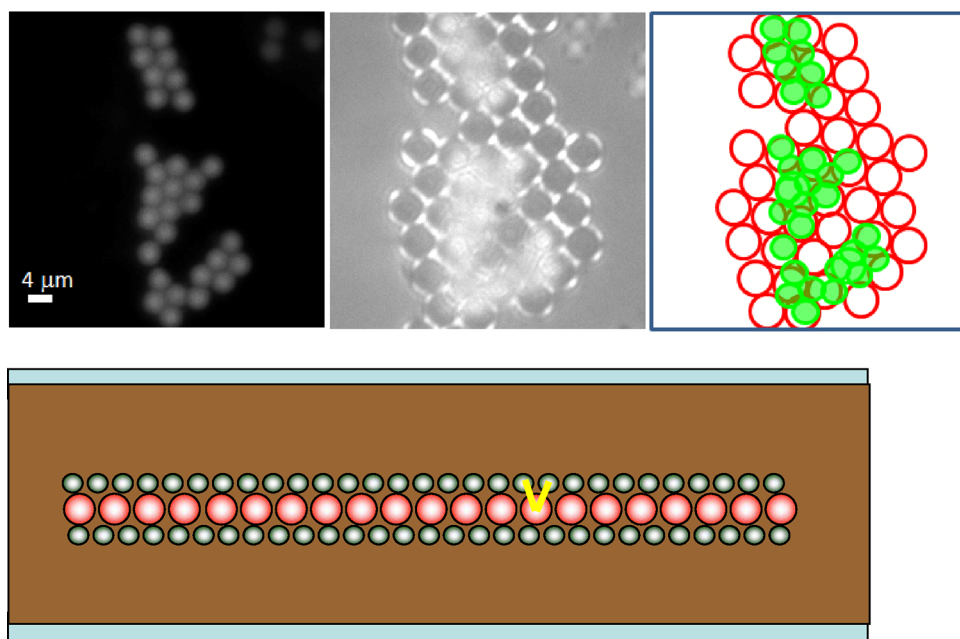


Figure 7. Fluorescence (top left) and polarization reflection microscope image (top middle) of an incommensurate crystalline phase $H_z = 0$ mT, $\Omega = 120$ s^{-1} , $H_{\parallel} = 1.82$ mT, $2a_d = 2.0$ μm (black). The top right picture shows a scheme of the packing of the paramagnets (red) and diamagnets (green). On the bottom, we have a side-view scheme of the incommensurate structure, where two paramagnetic-diamagnetic bonds that are partially frustrated are shown in yellow.

diluting the ferrofluid, we observe a slowing down of the large-scale diffusion that eventually stops completely. For a bead diameter $a_d = 2.0 \mu\text{m}$, the diamagnets remain on top and below the paramagnetic particle where they reside (Figure 6). In the

plot of the mean-square displacement of the diamagnetic beads in Figure 4, we observe a much weaker increase of the mean-square displacement with time that eventually settles at roughly 1% of the area of a paramagnetic unit cell. According to the

Lindemann criterion, a crystal should melt when the root-mean-square displacements of its elements amount for $1/10$ of the lattice spacing. We would, hence, expect a diamagnetic crystal to immediately melt under the current conditions. It is, however, not the interactions between the diamagnets but the interaction with the crystal potential of the paramagnets that causes the crystalline order of the diamagnets. The diamagnets are, hence, enslaved by the paramagnetic crystal, and they form two crystal layers growing epitaxial with the same unit cell on the paramagnetic crystals.

Paramagnetic Crystal Incommensurate Diamagnetic

Crystal Phase. For larger densities of the diamagnets and when using concentrated ferrofluids, the attraction between the diamagnets overcomes the paramagnetic crystal potential, and the diamagnets form close-packed hexagonal crystals on top and below the paramagnetic close-packed hexagonal crystal that has its own unit cell turned by 30 degrees with respect to the paramagnetic unit cell. The close-packed cells of the paramagnetic and diamagnetic crystal layers have periodicities defined by the diameters of the paramagnetic and diamagnetic beads that generically are incommensurate. Figure 7 shows such an incommensurate crystal structure.

We also observe the formation of disordered structures when neither the interdiamagnetic interaction nor the interaction of the diamagnets with the paramagnets dominates. Under such circumstances, diamagnets may form small close packed incommensurate clusters on top of the perfectly ordered paramagnet that follow the periodicity of the paramagnetic lattice on a larger scale.

5. DISCUSSION

The structure of the phases observed can all be understood by considering the time-averaged dipolar interactions between the constituents (eq 7). Depending on the precession angle of the external field, we expect paramagnets to bind to larger structures in bond angle directions that are attractive (violet in Figure 2). In this way, we obtain an assembly of paramagnets in the attractive bond directions $\vartheta_b^{\text{equi}}$, $\vartheta_b^{\text{anti}}$ that are all pointing with their magnetic moments in the same direction parallel to the external field. The order resembles a ferromagnetic ordering; however, the magnetic moments here are not permanent but are induced by the external field. We, hence, named the ordering a uniform ordering. The time-averaged dipole interaction between diamagnets behaves the same way creating a diamagnetic uniform order with the diamagnetic moments all pointing antiparallel to the magnetic field. Bonds between diamagnets and paramagnets are attractive in bond directions $\vartheta_b^{\text{anti}}$, $\vartheta_b^{\text{anti}}$ perpendicular to the equimagnetic bond directions. In those orthogonal directions (orange bond directions in Figure 2), we obtain a staggered order of alternating para- and diamagnets that resembles a ferrimagnet; however, the staggered magnetic moments are induced moments and not permanent moments.

The entire order, hence, consists of opposite magnetic particles that assemble in an alternating induced staggered sequence in one or two directions while the arrangement is uniform in the remaining directions. Whether the staggered ordering is in plane and the uniform order is normal to the film or the other way around is controlled by the precession angle ϑ_{ext} of the external magnetic field. Staggered equatorial ordering $\vartheta_b^{\text{anti}} > \vartheta_{\text{magic}}$ and uniform polar $\vartheta_b^{\text{equi}} < \vartheta_{\text{magic}}$ ordering is supported by precession angles $\vartheta_{\text{ext}} < \vartheta_{\text{magic}}$ below the magic angle, while uniform equatorial $\vartheta_b^{\text{equi}} < \vartheta_{\text{magic}}$ ordering and

staggered polar ordering $\vartheta_b^{\text{anti}} < \vartheta_{\text{magic}}$ is supported by angles $\vartheta_{\text{ext}} > \vartheta_{\text{magic}}$. It is for this reason that colloidal flowers form at $\vartheta_{\text{ext}} < \vartheta_{\text{magic}}$ while sandwich structures are stable for $\vartheta_{\text{ext}} > \vartheta_{\text{magic}}$. When the precession angle of the magnetic field is near magic $\vartheta_{\text{ext}} \approx \vartheta_{\text{magic}}$, we are in the regime where biaxial ordering prevails $|\alpha| > 1$ with uniform ordering along one equatorial direction $\varphi_b^{\text{equi}} = 0$, $\vartheta_b^{\text{equi}} > \vartheta_{\text{magic}}$ and with staggered ordering along the other equatorial direction $\varphi_b^{\text{anti}} = \pi/2$, $\vartheta_b^{\text{anti}} > \vartheta_{\text{magic}}$.

At large precession angles, we observe the equatorial uniform ordering with crystalline packing of the paramagnets and different types of packing of the diamagnets.

The gaseous and different crystalline diamagnetic structures are controlled by the strength of thermal fluctuations and the dipole interactions. Whether the dipole interaction between paramagnets or diamagnets or between diamagnets and paramagnets dominates can be controlled via the susceptibility contrasts, the size of the particles, and the volume fraction of both types of particles. The susceptibility contrasts can be changed by diluting the ferrofluid. Small particles are mobile and prefer gaseous phases; large particles are immobile. At low volume fractions of diamagnets ϕ_d in a diluted ferrofluid ($\chi_F \ll 1$), we may use the ferrofluid susceptibility as a small parameter. The interaction of the diamagnets with the paramagnets is stronger ($\propto \chi_F^{-1}$) than the interaction between them ($\propto \chi_F^2$). Each paramagnet binds one diamagnet to its north pole leaving diamagnetic bonds frustrated because the diamagnets are separated more than their close-packed distance. It is for such conditions where we observe the enslaved crystal phase. In concentrated ferrofluid at a high fraction of diamagnets, each paramagnet in the membrane can bind more than one diamagnet, and the diamagnetic dipole interaction becomes stronger, such that diamagnets form a close-packed membrane above the paramagnets as well. As a drawback, some of the diamagnets reside at positions with bond angles to the paramagnet that are suboptimal (Figure 7 bottom). In this limit, paramagnetic diamagnetic bonds are partially frustrated and incommensurate phases are observed.

We can estimate the amount of neutralization between the paramagnets and diamagnets by the excess susceptibility

$$\Delta\chi_{\text{eff}} = \frac{M^{\text{excess}}}{H_{\text{ext}}} = [\Delta\chi_p\phi_p + \Delta\chi_d\phi_d] \quad (8)$$

where ϕ_p and ϕ_d are the volume fractions of para- and diamagnets in the fluid. For our samples, we had $\Delta\chi_{\text{eff}} > 0$ such that interactions between paramagnets dominate all other dipole interactions. They hence formed structures they also would have formed without the presence of the diamagnets. The diamagnets, however, had to accept the distorted structure of the magnetic field generated by the paramagnets and had to arrange themselves accordingly. Presumably when using truly neutralizing mixtures $\Delta\chi_{\text{eff}} \approx 0$, the then more symmetric situation between para- and diamagnets would produce even more interesting superstructures. At present, we do not have ferrofluids of sufficient magnetic susceptibility to test such fully dipolar neutralized superstructures. However, even without having explored the full parameter space of possible structures, it is clear that the control of the different parameters in the dipole interaction of different particles as well as the control of the volume fraction of particles allows the construction a rich variety of phases in a mixed diamagnetic and paramagnetic system.

6. CONCLUSIONS

Staggered ordered colloidal phases with alternating arrangements of effectively diamagnetic and paramagnetic particles are formed in mixtures of paramagnetic and diamagnetic colloids immersed into a ferrofluid and are subject to a quickly varying time dependent magnetic field. Depending on the mean orientation of the time-averaged dyadic product of the external magnetic field, the staggered order is observed in the plane of the film in the form of colloidal flowers or normal to the film in the form of 2D paramagnetic crystals sandwiched between a diamagnetic gas or crystal. Near the magic angle, eccentricity of the modulation creates also biaxial structures. The order of the diamagnetic sandwich layer depends on a subtle balance of parameters entering into the dipole interactions at work between the different particles

■ AUTHOR INFORMATION

Corresponding Author

*E-mail: thomas.fischer@uni-bayreuth.de.

Notes

The authors declare no competing financial interest.

■ ACKNOWLEDGMENTS

We thank Thomas Friedrich for helping with susceptibility measurements of the ferrofluids. This work is supported by the German Science Foundation within the cluster of excellence SFB840.

■ REFERENCES

- (1) van Blaaderen, A.; Ruel, R.; Wiltzius, P. *Template-directed colloidal crystallization*. *Nature* **1997**, *385*, 321–324.
- (2) Li, F.; Josephson, D. P.; Stein, A. *Colloidal Assembly: The Road from Particles to Colloidal Molecules and Crystals*. *Angew. Chem., Int. Ed.* **2011**, *50*, 360–388.
- (3) Pieranski, P. *Colloidal crystals*. *Contemp. Phys.* **1983**, *24*, 25–73.
- (4) Paunov, V. N.; Cayre, O. J. *Supraparticles and "Janus" particles fabricated by replication of particle monolayers at liquid surfaces using a gel trapping technique*. *Adv. Mater.* **2004**, *16*, 788–791.
- (5) Perro, A.; Reculusa, S.; Ravaine, S.; Bourgeat-Lami, E. B.; Duguet, E. *Design and synthesis of Janus micro- and nanoparticles*. *J. Mat. Chem.* **2005**, *15*, 3745–3760.
- (6) Doye, J. P. K.; Louis, A. A.; Lin, I. C.; Allen, L. R.; Noya, E. G.; Wilber, A. W.; Kok, H. C.; Lyus, R. *Controlling crystallization and its absence: proteins, colloids and patchy models*. *Phys. Chem. Chem. Phys.* **2007**, *9*, 2197–2205.
- (7) Romano, F.; Sciortino, F. *Colloidal self-assembly: Patchy from the bottom up*. *Nat. Mater.* **2011**, *10*, 171–173.
- (8) Sutera, S. P.; Boylan, C. W. *Nearly monodisperse population of prolate ellipsoidal particles useful for colloidal research*. *J. Colloid Interface Sci.* **1980**, *73*, 295–297.
- (9) Nagy, M.; Keller, A. *Ellipsoidal polymer particles with predesigned axial-ratio*. *Polym. Commun.* **1989**, *30*, 130–132.
- (10) Glotzer, S. C.; Solomon, M. J. *Anisotropy of building blocks and their assembly into complex structures*. *Nat. Mater.* **2007**, *6*, 557–562.
- (11) Martin, J. E.; Venturini, E.; Gulley, G. L.; Williamson, J. *Using triaxial magnetic fields to create high susceptibility particle composites*. *Phys. Rev. E* **2004**, *69*, 021508.
- (12) Hynninen, A. P.; Dijkstra, M. *Phase diagram of dipolar hard and soft spheres: Manipulation of colloidal crystal structures by an external field*. *Phys. Rev. Lett.* **2005**, *94*, 138303.
- (13) Erb, R. M.; Son, H. S.; Samanta, B.; Rotello, V. M.; Yellen, B. B. *Magnetic assembly of colloidal superstructures with multipole symmetry*. *Nature* **2009**, *457*, 999–1002.
- (14) The continuity of the parallel component of the magnetic field and the normal component of the magnetic induction follow directly from the magnetostatic Maxwell equations. See, e.g., Feynman, R. P.; Leighton, R. B.; Sands, M. *The Feynman Lectures on Physics*, 6th ed.; Addison Wesley, 1977; Vol. 2.
- (15) Gast, A. P.; Zukoski, C. F. *Electrorheological fluids as colloidal suspensions*. *Adv. Colloid Interface Sci.* **1989**, *30*, 153.
- (16) Osterman, N.; Poberaj, I.; Dobnikar, J.; Frenkel, D.; Zherl, P.; Babic, D. *Field-Induced Self-Assembly of Suspended Colloidal Membranes*. *Phys. Rev. Lett.* **2009**, *103*, 228301.
- (17) Ray, A.; Aliaskarishohi, S.; Fischer, Th. M. *Dynamics of self-assembly of flower-shaped magnetic colloidal clusters*. *Phys. Rev. E* **2010**, *82*, 031406.
- (18) Ray, Ayan Fischer, Th. M. *Core size effects on the rotation and stability of dipolar clusters in precessing magnetic fields*. *Eur. Phys. J. E* (in print).